CHEMISTRY
A EUROPEAN JOURNAL

DOI: 10.1002/chem.200801864

Solid-Phase Synthesis of Peptide Libraries Combining α-Amino Acids with Inorganic and Organic Chromophores

Katja Heinze*[a] and Klaus Hempel[b]

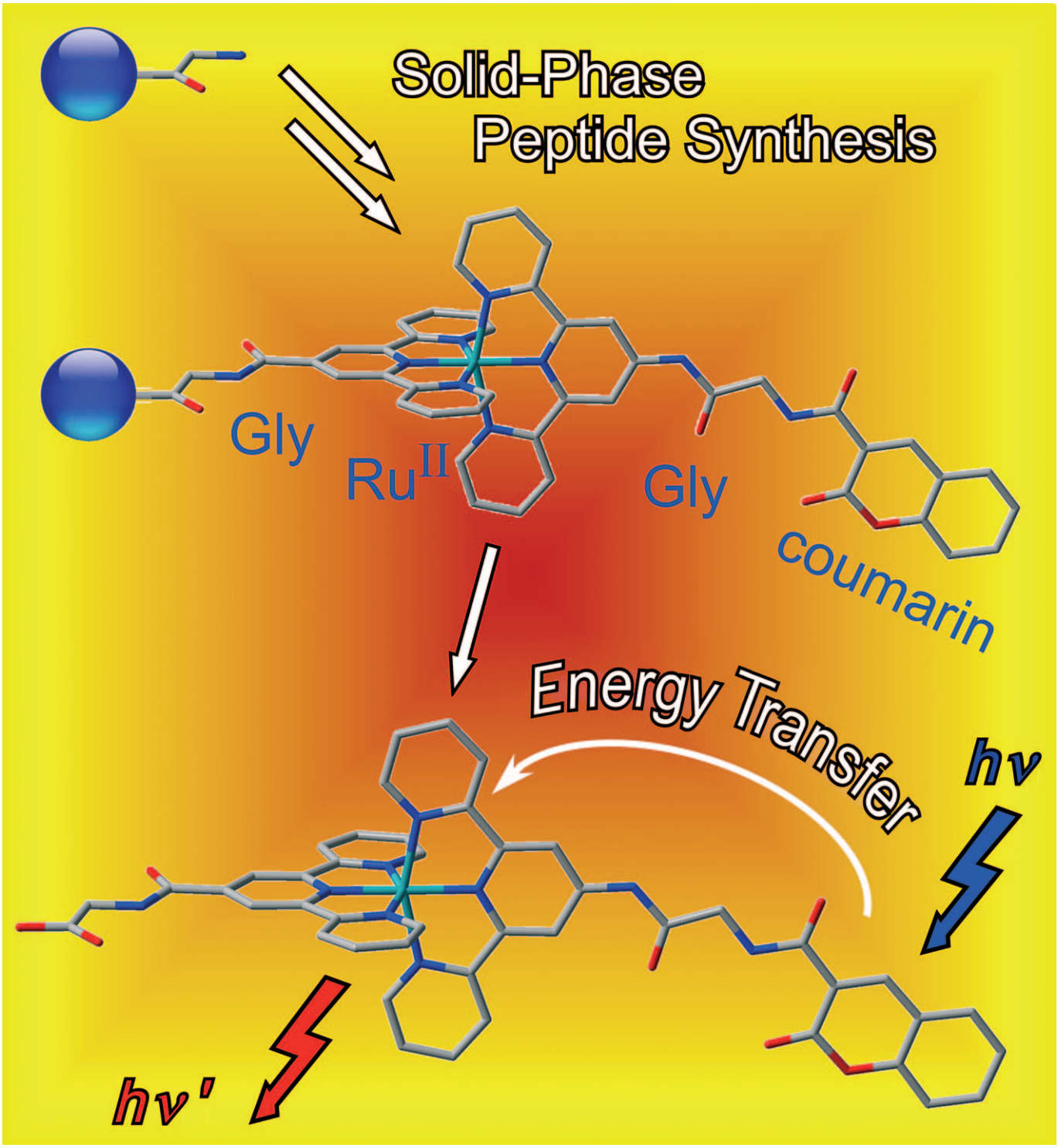

Abstract: The synthesis of two series of peptidic chains composed of bis(terpyridine)ruthenium(II) acceptor units and organic chromophores (coumarin, naphthalene, anthracene, fluorene) by stepwise solid-phase peptide synthesis (SPPS) techniques is described. The first series of dyads comprises directly amide linked chromophores, while the second one possesses a glycine spacer between the two chromophores. All dyads were studied by UV/Vis and NMR spectroscopy, steady-state luminescence, luminescence decay and electrochemistry, as well as by DFT calculations. The results of these studies indicate weak electronic coupling of the chromophores in the ground state. Absorpion spectra of all dyads are dominated by metal-to-ligand charge-transfer (MLCT) bands around 500 nm. The bichromophoric systems, especially with coumarin as organic chromophore, display additional strong absorptions in the visible spectral region. All complexes are luminescent at room temperature (^{3}MLCT). Efficient quenching of the fluorescence of the organic chromophore by the attached ruthenium complex is observed in all dyads. Excitation spectra indicate energy transfer from the organic dye to the ruthenium chromophore.

Keywords: energy transfer · light harvesting · peptides · ruthenium · solid-phase synthesis · terpyridine

Introduction

Over the last decades ruthenium–polypyridyl complexes have attracted particular attention due to their interesting and potentially useful photophysical properties.[1,2] The parent complex $[Ru(bpy)_3]^{2+}$ (bpy = 2,2′-bipyridine) possesses a long-lived emissive triplet state at room temperature, which is important for applications in practical devices that rely on solar energy, such as dye-sensitised solar cells (DSSCs).[3–6] However, $[Ru(bpy)_3]^{2+}$ has only a weak absorbance in the red part of the solar spectrum ($\lambda_{max} \approx 450$ nm)[7] so intense research efforts have been devoted to the extension of the absorption window of such complexes.[8–11] $[Ru(tpy)_2]^{2+}$ (tpy = 2,2′:6,2″-terpyridine) complexes feature a bathochromically shifted absorption band around $\lambda_{max} = 500$ nm. However, these complexes are usually almost non-emissive at room temperature. In fact, the parent $[Ru(tpy)_2]^{2+}$ complex has a very short-lived excited ^{3}MLCT state and subsequently a very low quantum yield at room temperature in fluid medium.[12] One possibility to enhance the excited-state properties of $[Ru(tpy)_2]^{2+}$ complexes is to substitute the terpyridine ligands on the 4′-positions with electron-donating or -withdrawing groups.[13–15] For example, $[Ru(tpy)(tpy\text{-}COOEt)]^{2+}$ emits at 667 nm with a quantum yield of 2.7×10^{-4} and $\tau = 32$ ns at 298 K in acetonitrile.[15]

In addition heteroleptic $[Ru(tpy\text{-}R)(tpy\text{-}R')]^{2+}$ complexes with substituents in 4′-position are non-stereogenic in contrast to the trischelate complexes based on $[Ru(bpy)_3]^{2+}$, thus facilitating synthesis and purification and still offering the possibility for functionalisation. Thus heteroleptic $[Ru(tpy\text{-}R)(tpy\text{-}R')]^{2+}$ complexes are also attractive components of dyads incorporating organic chromophores with intense molar absorptivity in the UV/visible spectral region.[16–23]

Recently, we have introduced a heteroleptic $[Ru(tpy\text{-}R)(tpy\text{-}R')]^{2+}$ complex with R = COOH and R′ = NH_2 giving metallo amino acid **1d**, which places the metal centre in between the functional groups.[27] This feature is exclusive for **1d**, in contrast to other ruthenium containing amino acids reported so far (**1a**,[24] **1b**[25] and **1c**[26]) with ruthenium located at the side-chain. Incorporation of ruthenium in the main chain of a peptide as opposed to peptides modified at the side chain should give rise to enhanced electronic communication between building blocks. Indeed, ferrocene derivatives have been successfully coupled to the artificial amino acid **1d** through amide bonds either at the *N*- or at the *C*-terminus and photo-induced electron transfer (PET) has

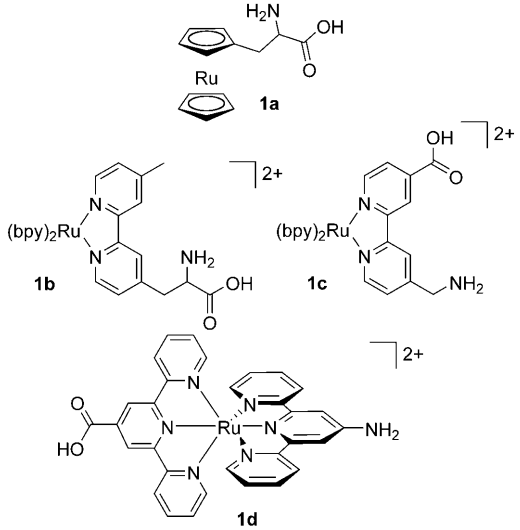

[a] Prof. Dr. K. Heinze
Institute of Inorganic Chemistry and Analytical Chemistry
Johannes Gutenberg-University of Mainz
Duesbergweg 10–14, 55128 Mainz (Germany)
Fax: (+49) 6131-39-27277
E-mail: katja.heinze@uni-mainz.de

[b] Dipl.-Chem. K. Hempel
Department of Inorganic Chemistry
University of Heidelberg, Im Neuenheimer Feld 270
69120 Heidelberg (Germany)

Supporting information for this article is available on the WWW under http://dx.doi.org/10.1002/chem.200801864. It contains tables of ^{1}H NMR and ^{13}C NMR data; DFT optimised Cartesian Coordinates of **2a–2d**, **3a–3f**.

been observed, provided the redox potential of the ferrocene unit is energetically below the excited-state redox potential of the ruthenium moiety.[27]

An artificial peptide containing $[Ru(tpy)_2]^{2+}$ units (**1e**) was designed and prepared by Ueyama et al. using stepwise complex formation and amide coupling reactions.[28] Right-handed helical peptides with up to five ruthenium moieties were obtained. However, the metal centres do not exhibit a significant electronic communication due to the separation with leucine spacers.

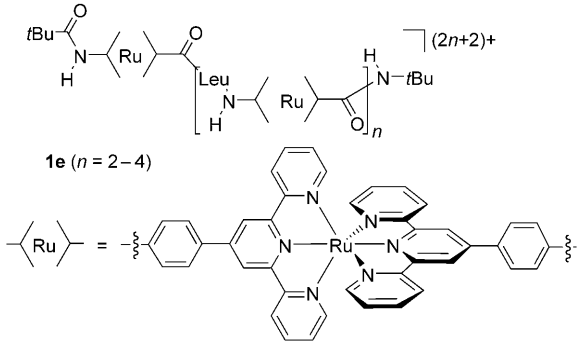

Metallo amino acids are in principle amenable to solid-phase peptide synthesis (SPPS) procedures, which would allow preparing multifunctional systems, such as multichromophore arrays, by parallel synthetic processes. This is especially advantageous when several reaction steps are necessary and when high yields and high purity should be achieved with minimal effort. Solid-phase synthesis with metal complexes is a relative new field and has been recently reviewed from different perspectives.[29,30,31] For example, 1) a series of trisheteroleptic ruthenium(II) complexes has been recently prepared by solid-phase methods by Meggers for potential application as acetylcholinesterase inhibitors,[32] 2) peptide-tethered platinum(II) complexes for use as cytostatic drugs have been prepared by automated parallel solid-phase synthesis by van Boom and Reedijk,[33] 3) a library of iridium(III) acetylacetonato complexes has been synthesised by Li as red-phosphorescent emitters in organic light-emitting diodes (OLEDs)[34] and 4) ferrocene-incorporating peptides have been constructed by SPPS techniques by Metzler-Nolte and Heinze.[35,36]

In this work we extend the SPPS approach to incorporate the artificial metallo amino acid **1d** into multichromophore systems with suitably substituted organic dyes (coumarins, naphthalene, anthracene, fluorene). The aim is to develop a fast, simple and reliable high-throughput technique for synthesising and screening of potential light-harvesting arrays.

Results and Discussion

Strategy: The functionalisation of photoactive compounds requires a synthetic strategy that results in products of high purity, as photoactive byproducts might dramatically disturb the results of photophysical assays.

Especially, when several synthetic steps are necessary, an accurate workup after each step is absolutely essential. SPPS allows the use of an excess of starting materials to give full conversion and furnishes a simple workup by just washing and filtration of the insoluble support. Thus the SPPS technique is employed for the synthesis of dyads.

Building block synthesis: The Ru-containing amino acid **1d** was prepared by reaction of $[RuCl_3(tpy\text{-}COOEt)]$ with tpy-NH_2 in a microwave synthesiser at 120 °C in ethanol and subsequent ester hydrolysis in 20% sulphuric acid at 100 °C.[27] This harsh procedure underlines the high stability of these $[Ru(tpy)_2]^{2+}$ complexes. Acid chlorides of the organic dyes (R–COCl) were prepared by heating the respective carboxylic acids in a $THF/CH_2Cl_2/SOCl_2$ mixture followed by recrystallisation from a solution of the acid chloride in CH_2Cl_2 by addition of an excess hexane.[37]

Solid-phase synthesis of 2a–2d and 3a–3f: First attempts to directly couple **1d** as an ester to standard polystyrene/divinylbenzene resins with Wang linkers were unsuccessful, since in our hands these resins could not be completely loaded possibly due to the bulkiness of the $[Ru(tpy)_2]^{2+}$ complex **1d**.

Thus a TentaGel S resin with a Wang linker was used, which is distinguished by lower loading and higher flexibility of the polymer chains as well as better swelling properties.[38,39] As a spacer between resin-bound polyethylene glycol chains (PEG) and target molecules, a glycine unit was attached to the resin through an ester group (Scheme 1).

To accomplish this Fmoc-protected (Fmoc = 9-fluorenylmethoxycarbonyl) glycine was coupled to the resin by addition of exess Cl-Gly-Fmoc to the washed and swollen resin and shaking the reaction mixture in an overhead shaker for 2 h (Scheme 1).[40] After washing the resin with CH_2Cl_2 for three times, deprotection in a piperidine/CH_2Cl_2 mixture and again washing with CH_2Cl_2 for three times, a solution of pre-activated [pyridine, PyBOP = benzotriazole-1-yl-oxy-tris(dimethylamino)phosphonium hexafluorophosphate] metallo amino acid **1d** in acetonitrile was poured to the resin and the suspension was shaken for 12 h.

Notably, protection of the amine substituent of **1d** is unnecessary as tpy-NH_2 is a very poor nucleophile. This is even aggravated when tpy-NH_2 is coordinated to the ruthenium dication. On the other hand this NH_2 group requires activation by strong bases, for example, phosphazene base P_1-*t*Bu (P_1-*t*Bu = *tert*-butyliminotris(dimethylamino)phosphorane),[27] or very strong electrophiles such as acid chlorides have to be employed for successful amide coupling.[41] In our hands the presence of $[Ru(tpy)_2]^{2+}$ and phosphazene base P_1-*t*Bu causes partial cleavage of PEG chains of the TentaGel resin. Thus it proved to be more favourable to use acid chlorides instead of strong bases to couple acetyl, coumarinyl, naphthylmethylenyl, trifluoro acetyl (**2a–2d**) and glycinyl moieties (**3f**) to the NH_2 group of resin bound **1d** (Scheme 1).

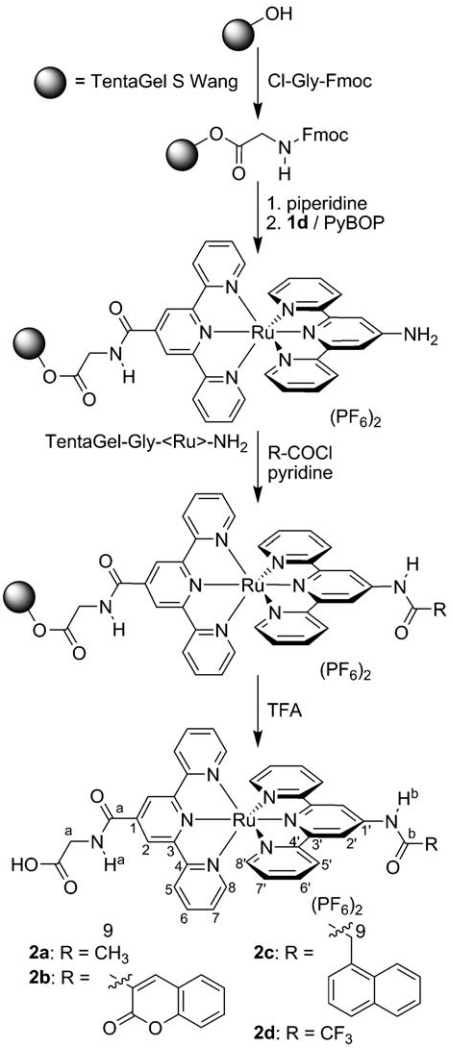

Scheme 1. Solid-phase synthesis of conjugates **2a**–**2d** (PyBOP = (benzotriazole-1-yloxy)tripyrrolidinophosphonium hexafluorophosphate, Fmoc = 9-fluorenyl-methoxycarbonyl, TFA = trifluoroacetic acid) and partial atom numbering.

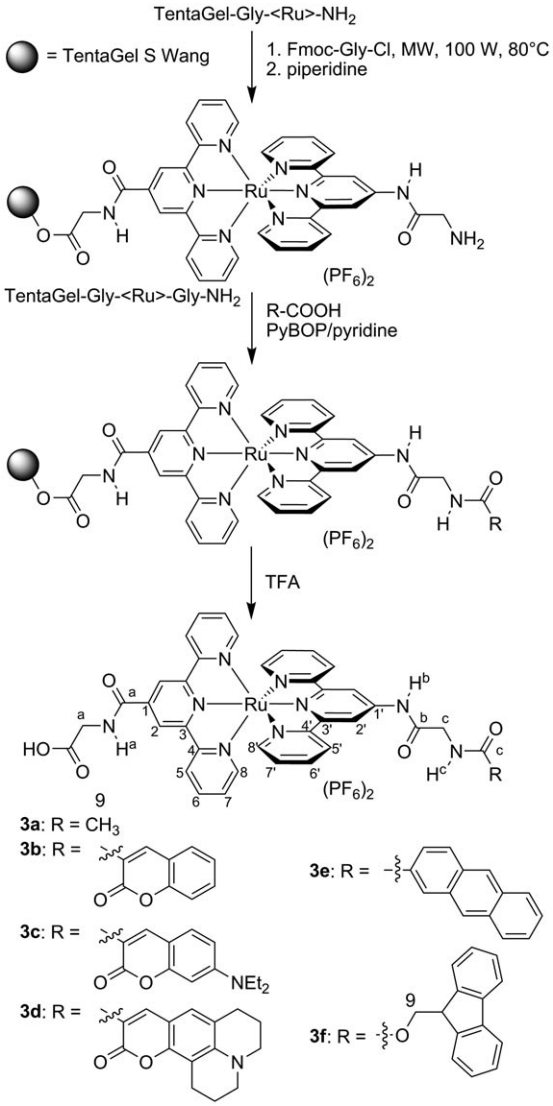

Scheme 2. Solid-phase synthesis of conjugates **3a**–**3f** and partial atom numbering.

For compounds **2a**–**2d** this was accomplished by shaking TentaGel-Gly-⟨Ru⟩-NH_2 for 12 h with a solution of the respective acid chloride (2.5–3.2 equiv) and pyridine, to scavenge released hydrochloric acid. Again the resin was washed several times before compounds **2a**–**2d** were cleaved from the resin by treatment with trifluoro acetic acid. Conjugates **2a**–**2d** were obtained by precipitation from an aqueous solution by addition of NH_4PF_6 in 73–80 % yield.

The second series features a glycine spacer between the ruthenium complex and the organic dye (Scheme 2). As Cl-Gly-Fmoc appeared to be quite unreactive with respect to immobilised **1d**, the reaction mixture of TentaGel-Gly-⟨Ru⟩-NH_2 and Cl-Gly-Fmoc was advantageously heated in a microwave synthesiser in absolute THF to 80 °C for 1 h.[42] To obtain compounds **3a**–**3e** the Fmoc protection group of TentaGel-Gly-⟨Ru⟩-Gly-Fmoc was removed by piperidine to give TentaGel-Gly-⟨Ru⟩-Gly-NH_2. The resulting NH_2 group of the glycine was much more reactive than the tpy-NH_2 group, but also more sensitive towards decomposition. Thus milder coupling reagents than acid chlorides were required and the PyBOP/pyridine strategy[40] was used to activate coumarinyl, coumarin-NEt_2-yl-, and coumarin343-yl moieties instead of activation as acid chlorides.

Due to the low solubility of anthracene-2-carboxylic acid in polar solvents, especially after deprotonation, the DCC/HOBt protocol (DCC = *N*,*N*′-dicyclohexylcarbodiimide, HOBt = 1-hydroxybenzotriazol) was employed. In all cases a solution of the pre-activated acid was poured to TentaGel-Gly-⟨Ru⟩-Gly-NH_2 and the mixture was shaken for 12 h. After washing and filtration compounds **3a**–**3e** were obtained by release from the resin with TFA and precipitation from an aqueous solution by addition of NH_4PF_6 in 33–80 % yield (Scheme 2). Compound **3f** was obtained analogously from TentaGel-Gly-⟨Ru⟩-Gly-Fmoc in 80 % yield.

Spectroscopic characterisation of 2a–2d and 3a–3f: Compounds **2a–2d** and **3a–3f** were characterised by ESI and HR-ESI mass spectrometry; ^{1}H NMR, ^{13}C NMR and IR spectroscopy; and elemental analysis.

The composition of all compounds was verified by ESI mass spectrometry. As all complexes contain a Ru^{2+} ion, the spectra show molecular peaks at $M/2$ with the isotope distribution of a dication. The spectra also evidenced the purity of the samples as no other charged ruthenium containing species were observed. Furthermore HR-ESI spectra prove the molecular formulae of all compounds (see Experimental Section).

Proton NMR spectra of **2a–2d** and **3a–3f** are quite similar and the data are listed in Tables S1–S3 (Supporting Information).

As an example the ^{1}H NMR spectrum of the coumarin-NEt_2 derivative **3c** is shown in Figure 1. Generally, amide bond formation at NH^b is substantiated by the significant shift of $H^{2'}$ from around $\delta = 8$ ppm in the free amine[27] to $\delta = 9$ ppm in the products. The two doublets of the methylene protons of the two glycine moieties in **3c** are observed at $\delta = 4.29$ ppm for CH^a and $\delta = 4.45$ ppm for CH^c.

Distinguishing CH^a and CH^c was accomplished by HSQC spectroscopy. Exemplary, the HSQC spectrum of **3c** clearly shows cross peaks between the methylene protons of the glycine moieties CH^a and CH^c and the respective amide protons NH^a and NH^c (Figure 2), proving the successful incorporation of two glycine moieties in compounds **3a–3f**.

In **3c** the three expected amide proton signals are found at $\delta = 8.29$ (NH^a), 9.35 (NH^c) and 10.05 ppm (NH^b). While the signal of NH^a appears in the expected range, the signals of NH^b and NH^c are dramatically shifted to lower field. In case of NH^b this is due to the electron-withdrawing effect of the adjacent cationic complex. In case of NH^c an intramolecular hydrogen bond of NH^c to the carbonyl group of the coumarin moiety is possible. All coumarin-containing compounds (**2b**, **3b–3d**) show this hydrogen bond between the amide proton and the lactone carbonyl oxygen atom as NH^b (**2b**) and NH^c (**3b–3d**) resonate at very low field.

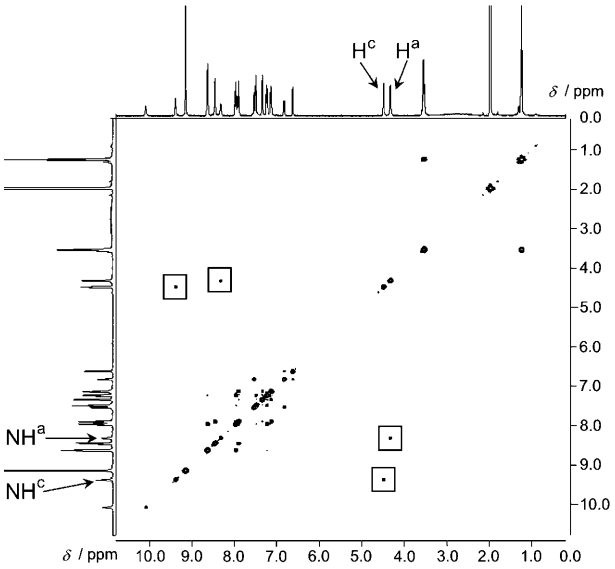

Figure 2. HSQC spectrum of **3c** in CD_3CN.

All remaining proton signals of the terpyridine ligands and the respective chromophores appear in the expected chemical shift ranges and confirm the correct attachment of the organic dyes.

The ^{13}C NMR spectra of **2a–2d** and **3a–3f** show all expected signals including those for the quarternary carbon atoms, all carbonyl carbon atoms and the carboxylic acid carbon atom. All ^{13}C NMR data are listed in Tables S4 and S5 (Supporting Information). Assignments were performed by using 2D NMR correlation spectroscopy.

In the IR spectra of the conjugates **2a–2d** and **3a–3f** bands at around $\nu = 843$ cm^{-1} are assigned to the P–F vibration of the PF_6^- counterions. Bands at 1219–1230 cm^{-1} correspond to C–O stretching vibrations and bands at 1702–1733 cm^{-1} to those of the C=O stretching vibration of the carboxylic acid moieties. The amide groups cause absorptions at 1615–1693 (amide I) and 1521–1538 cm^{-1} (amide II).[43] Furthermore, bands for the C=N and C=C bonds at 1571–1614 cm^{-1} are observed while C–H stretching vibration bands are found at around 2930 (CH_{alkyl}) and

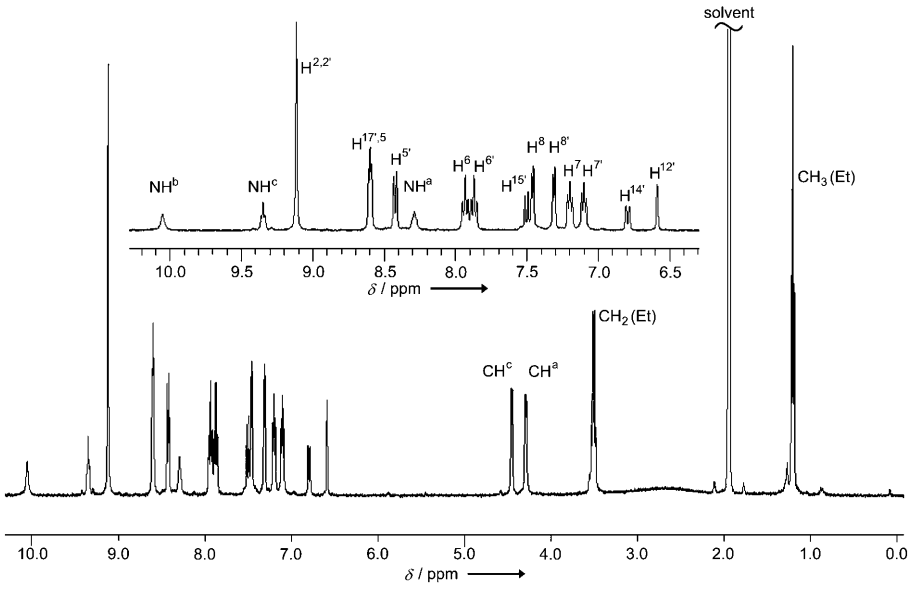

Figure 1. ^{1}H NMR-spectrum of **3c** in CD_3CN.

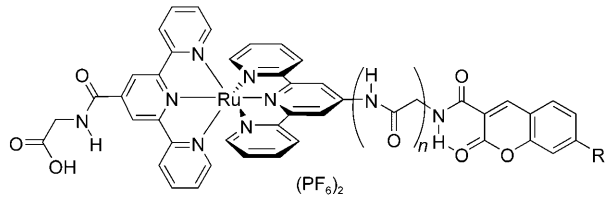

2b : R = H, *n* = 0
3b : R = H, *n* = 1
3c : R = NEt_2, *n* = 1
3d : R = N–$(CH_2)_3$–, *n* = 1

3075 cm^{-1} (CH_{aryl}). Unfortunately, absorption bands of O–H and N–H bonds emerge as very broad bands around 3445 cm^{-1} preventing further interpretation concerning hydrogen bonding.

Electrochemical properties of 2a–2d and 3a–3f: All electrochemical studies were performed in dry degassed acetonitrile with $nBu_4NB(C_6F_5)_4$ (0.1 M) as the supporting electrolyte, as this counterion solubilises highly charged species better than hexafluorophosphate salts[44] (Table 1). Figure 3 depicts the cyclic voltammogram of the coumarin-NEt_2 derivative **3c** as an example. All compounds are reversibly oxidised at around 1.3 V versus SCE. This oxidation is assigned to the ruthenium(II/III) couple, which appears rather insensitive to the attached chromophore or substituent. The coumarin-NR_2 derivatives **3c** and **3d** show an additional reversible oxidation at 1.12 and 0.90 V, respectively, which is caused by the oxidation of the dialkyl amino moiety attached to the coumarin chromophore. The terpyridine ligands are irreversibly reduced at around −0.8 and −1.2 V, except for the CF_3 derivative **2d**, which is already reduced at −0.45 V due to the electron-withdrawing nature of the CF_3 group. Compounds **2b**, **2c**, **3b**, **3c**, **3e** and **3f** show irreversible peaks for the reduction of the chromophores at lower potential, while the coumarin343 derivative **3d** displays only one broad irreversible peak at −1.29 V (Table 1).

Table 1. Electrochemical data[a] of complexes **2a–2d** and **3a–3f**.

	$E_{1/2}$ (Ru^{II}/Ru^{III})	$E_{1/2}$ (tpy/tpy$^-$)	$E_{1/2}$ (chromophore)
2a	1.285	−0.850, −0.945[b]	
2b	1.320	−0.760, −1.195[b]	−1.495[b]
2c	1.300	−0.830, −0.975[b]	−1.185[b]
2d	1.250	−0.445, −1.360[b]	
3a	1.295	−0.940, −1.150[b]	
3b	1.295	−0.945, −1.235[b]	−1.300[b]
3c	1.310	−0.825, −0.970[b]	1.120, −1.270[b]
3d	1.320	−1.295[b]	0.900, −1.365[b]
3e	1.305	−1.045, −1.155[b]	
3f	1.270	−0.845[b]	−1.090

[a] In $CH_3CN/nBu_4NB(C_6F_5)_4$; scan rate 200 $mV s^{-1}$; $E_{1/2}$ in V versus SCE. [b] Irreversible peak.

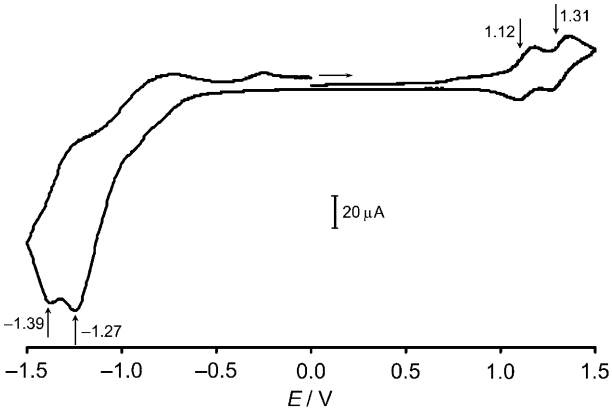

Figure 3. Cyclic voltammogram of **3c** in acetonitrile, $nBu_4NB(C_6F_5)_4$ (0.1 M) versus SCE.

Absorption and emission spectroscopy of 2a–2d and 3a–3f: The absorption spectra of all compounds show a characteristic band in the visible region at λ_{max} = 488–492 nm insensitive of the substituents R (Schemes 1 and 2, Figures 4 and 5, Table 2). This absorption is assigned to a metal-to-ligand charge transfer (MLCT) from the ruthenium centre to the terpyridine ligands.[13] The terpyridine ligands itself display absorption bands at λ_{max} = 308–310 and 275 nm ($\pi \rightarrow \pi^*$ transitions), respectively.[13] Coumarin- and naphthalene-containing **2b** and **2c**, respectively, additionally show absorption bands of the chromophores in the UV region at λ_{max} = 332

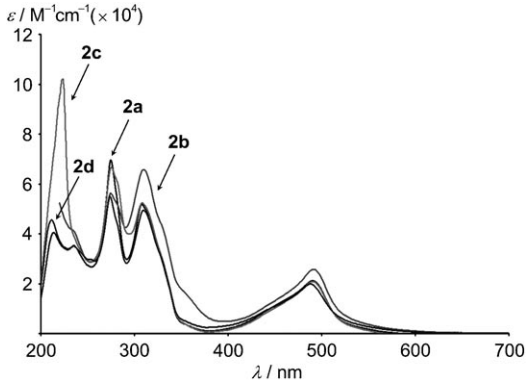

Figure 4. UV/Vis spectra of **2a–2d** in CH_3CN.

Table 2. UV/Vis data[a] of complexes **2a–2d** and **3a–3f**.

	MLCT: λ_{max} [nm] (ε [$M^{-1}cm^{-1}$])	terpyridine ($\pi \rightarrow \pi^*$): λ_{max} [nm] (ε [$M^{-1}cm^{-1}$])	chromophore ($\pi \rightarrow \pi^*$): λ_{max} [nm] (ε [$M^{-1}cm^{-1}$])
2a	490 (21150)	308 (51700); 275 (59500)	
2b	492 (25750)	310 (65720); 275 (56240)	332 (40290)
2c	490 (20810)	308 (52430); 275 (66650)	224 (102080)
2d	488 (19868)	309 (37820); 275 (41620)	
3a	490 (22290)	309 (55010); 275 (78270)	
3b	490 (26180)	307 (73120); 275 (80500)	328 (46290)
3c	490 (24950)	308 (56380); 275 (76080)	422 (47350)
3d	490 (25820)	308 (58260); 275 (79660)	441 (49090)
3e	491 (25830)	308 (64440); 274 (124540)	390 (6750); 258 (119810)
3f	490 (20590)	308 (49370); 275 (75910)	n.o[b]

[a] In CH_3CN. [b] n.o. = not observed.

and 224 nm.[45,18] Analogous to **2b**, the unsubstituted coumarin moiety in **3b** causes an absorption band at $\lambda_{max}=$ 328 nm,[45] while the bands of substituted coumarins are shifted to lower energy ($\lambda_{max}=422$ (**3c**)[46] and 441 nm (**3d**);[47] Figure 5). The anthracene conjugate **3e** absorbs at $\lambda_{max}=390$ and 258 nm (Figure 5).[23] Thus it appears that the spectra of the dyads are simply the superpositions of the component spectra indicating electronically decoupled chromophores in the ground state.

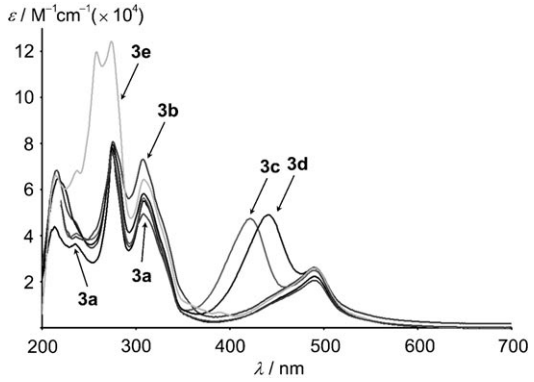

Figure 5. UV/Vis spectra of **3a**–**3f** in CH_3CN.

The steady-state luminescence spectra of **2a**–**2d** and **3a**–**3f** have been recorded at room temperature in acetonitrile. The pertinent data are summarised in Table 3. As expected all the heteroleptic ruthenium complexes display an emission centred around $\lambda_{max}=665$–671 nm when irradiated into the MLCT absorption maximum around $\lambda_{exc}=490$ nm with quantum yields (ϕ) around 5×10^{-4}, which is similar to the emission observed for $[Ru(tpy)(tpy\text{-}COOEt)]^{2+}$ ($\lambda_{max}=$ 667 nm; $\phi=2.7\times10^{-4}$).[15] The emission is attributed to ^{3}MLCT states of the $[Ru(tpy)_2]^{2+}$ unit.

From the absorption spectrum of dye-free **2a** (Figure 4) an absorption gap ranging approximately from 330–450 nm is evident. In fact only the tail of the terpyridine $\pi\rightarrow\pi^*$ absorption bands provide some extinction in this spectral window.

When **2a** is irradiated in this region ($\lambda_{exc}=340$ nm) the ruthenium-based ^{3}MLCT emission is also observed, but with reduced intensity relative to the MLCT excitation with $\lambda_{exc}=$ 493 nm (Figure 6). The same experiment using the coumarin-containing dyad **2b** yields almost the full ruthenium-based ^{3}MLCT emission intensity (Figure 6). This finding suggests energy transfer from the coumarin chromophore to the ruthenium unit in dyad **2b**.

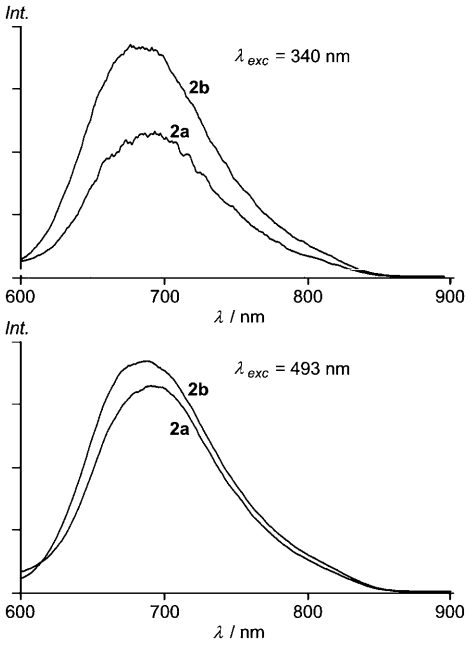

Figure 6. Emission spectra of **2a** and **2b** excited at $\lambda_{exc}=340$ and 493 nm in CH_3CN.

Coumarin conjugates **3b**–**3d** with a glycine spacer between the chromophores also exhibit sensitised emission from the chromophore, which is clearly evidenced from the excitation spectra when compared to that of coumarin-free **3a** (Figure 7). Evidently, the energy gap of the absorption and excitation spectra of **3a** is filled by the coumarin antenna in **3b**–**3d** (Figures 5 and 7).

Conversely the fluorescence emission of the antenna is strongly quenched by the appended ruthenium complex as the residual fluorescence of the antenna corresponds to less than 7% for **2b**, **2c**, **3b**, **3c** and **3d** of the luminescence intensity of the respective chromophore itself (Table 3). In the anthracene derivative **3e** only 78% of the anthracene fluorescence intensity is quenched by the ruthenium moiety, which might be due to an unfavourable relative orientation of the donor and acceptor chromophores in **3e** (see DFT calculation below).

To exclude an intermolecular quenching process, fully protected **1d** (the acid group as

Table 3. Photophysical data of complexes **2a**–**2d** and **3a**–**3f** in CH_3CN.

	λ_{max}(^{3}MLCT) [nm]	λ_{max} (chromophore) [nm]	ϕ(^{3}MLCT) (λ_{exc} [nm])	fluorescence quenching efficiency [%]
2a	671		9.28×10^{-4} (455)	
2b	668	405	9.19×10^{-4} (455)	93.6
2c	664	377	6.42×10^{-4} (463)	99.1
2d	666		6.30×10^{-4} (471)	
3a	670		6.14×10^{-4} (468)	
3b	667	401	5.41×10^{-4} (435)	99.6
3c	665	462	4.99×10^{-4} (459)	98.1
3d	665	478; 518	8.52×10^{-4} (468)	99.7
3e	666	413	1.05×10^{-3} (435)	78.4
3f	667		6.99×10^{-4} (463)	

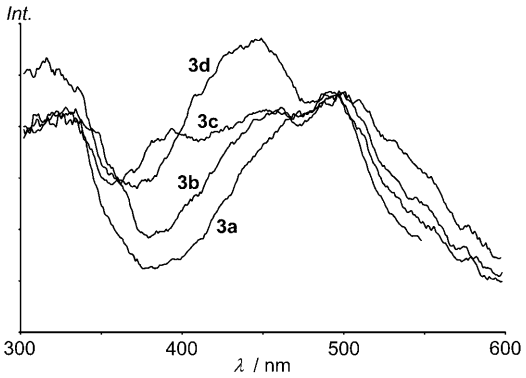

Figure 7. Excitation spectra of compounds **3a–3d** ($\lambda_{obs}=667$ nm) in CH_3CN.

ethyl ester; the amino group as acetyl amide, $\mathbf{1d^{EAc}}$) was titrated with 7-(diethylamino)coumarin-3-carboxylic acid in CH_3CN and the emission spectra upon excitation with $\lambda_{exc}=$ 422 and 490 nm were recorded. Almost no ruthenium-based ^{3}MLCT emission is observed when the mixtures are excited at 422 nm, while the coumarin fluorescence is fully conserved. In contrast the ruthenium-based emission is observed in dyad **3c** with maximum intensity and the coumarin fluorescence is largely quenched when excited at 422 nm (Figure 8).

In all cases, photoinduced energy transfer from the antenna singlet states to the ruthenium ^{1}MLCT state is thermodynamically feasible (singlet–singlet energy transfer pathway followed by intersystem crossing of the ^{1}MLCT to the ^{3}MLCT state) as is the potential triplet–triplet energy transfer from antenna triplet states (possibly populated by an enhanced intersystem crossing from the antenna singlet state due to the proximity of the heavy ruthenium atom) to the ^{3}MLCT state. However, the latter pathway seems to be more unlikely as the ruthenium atom is quite far away in systems with the glycine spacer **3b**, **3c**, **3d** and **3e**. Thus intersystem crossing of the organic dye should be hampered and the large fluorescence quenching in **3b**, **3c** and **3d** cannot be accounted for by this triplet–triplet energy transfer pathway, which is inline with previous studies of comparable systems.[18,19]

In addition we note a broadening of the excitation spectra in the MLCT region when a glycine spacer is inserted between the ruthenium centre and the organic dye. Figure 9 illustrates this finding for the coumarin derivatives **2b** and **3b**, which has no parallel in the respective absorption spectra (Figures 4 and 5). Though we do not have a simple, straight-forward explanation for this behaviour we can speculate that this phenomenon might arise from different preferred conformations and aggregation modes in solution, which differ also in their energy-transfer characteristics. In general energy transfer is modulated by the distance and the relative orientation of the donor and acceptor in either of the two limiting mechanisms. The Förster dipole–dipole exchange mechanism relies on the relative orientation of the interacting dipoles, while the Dexter through-bond double-electron transfer is dependent on the orbitals of the bridging unit and their orientation.[19] Also triplet–triplet energy transfer can be modulated by the dihedral angle between interacting units.[48]

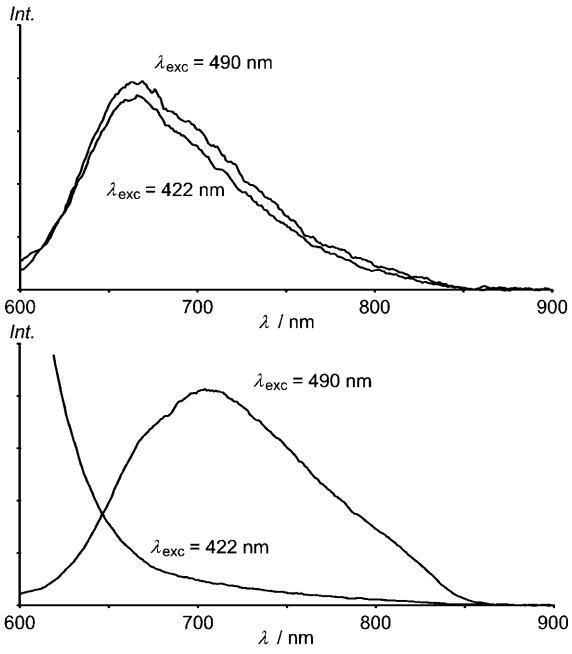

Figure 8. Emission spectra of **3c** (top) and a $\mathbf{1d^{EAc}}$/CoumarinNEt$_2$ mixture (1:1.5) (bottom) in CH_3CN.

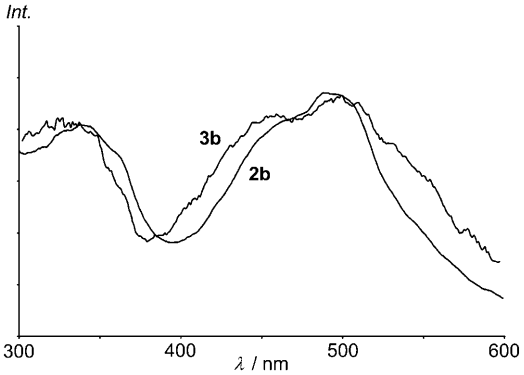

Figure 9. Excitation spectra of **2b** and **3b** in CH_3CN ($\lambda_{obs}=660$ nm).

Preliminary time-resolved luminescence studies were performed in deaerated acetonitrile by using a nanosecond time-correlated single-photon counting unit. Multiexponential decays were observed for acids **2a–2d** and **3a–3f** when excited at $\lambda_{exc}=500$, 450 or 370 nm (Table 4). To gain some insight into the excited state dynamics of the dyads the lifetimes of the amino acid **1d** and its ethyl ester $\mathbf{1d^E}$ were also determined. For the ester $\mathbf{1d^E}$ a monoexponential decay was observed ($\tau=33.7$ ns, $\lambda_{exc}=500$ nm, Figure 10) which matches that of $[Ru(tpy)(tpy\text{-}COOEt)]^{2+}$ ($\tau=32$ ns[15]), while the acid **1d** shows a biexponential decay ($\tau_1=26.3$, $\tau_2=3.5$ ns,

Table 4. Time-resolved luminescence data of **2a–d** and **3-a-f** in acetonitrile.

	τ (λ_{exc} = 500 nm) [ns] (fraction [%])	τ (λ_{exc} = 450 nm) [ns] (fraction [%])	τ (λ_{exc} = 370 nm) [ns] (fraction [%])
1d^{E}	33.7 (100)		
1d	26.26 (61.7) 3.45 (38.3)		
2a	18.0 (8.4) 3.9 (91.6)		
2b	17.4 (7.1) 2.7 (92.9)		19.2 (0.9) 3.4 (16.1) 0.5 (83.0)
2c	19.2 (8.3) 3.8 (91.7)		
2d	20.8 (18.0) 2.1 (82.0)		
3a	19.0 (5.0) 4.0 (95.0)		
3b	17.8 (8.9) 3.2 (91.1)		22.5 (1.4) 3.9 (26.0) 0.8 (72.6)
3c	15.1 (2.3) 3.7 (40.4) 0.4 (57.3)	15.2 (3.0) 4.0 (63.2) 0.8 (33.8)	
3d	19.3 (0.6) 3.4 (10.9) 0.5 (88.5)	20.9 (0.8) 3.5 (93.5) 0.8 (5.7)	
3e	22.0 (9.4) 3.8 (90.6)		18.4 (1.9) 9.1 (60.0) 1.2 (38.1)
3f	19.1 (12.9) 3.9 (87.1)		

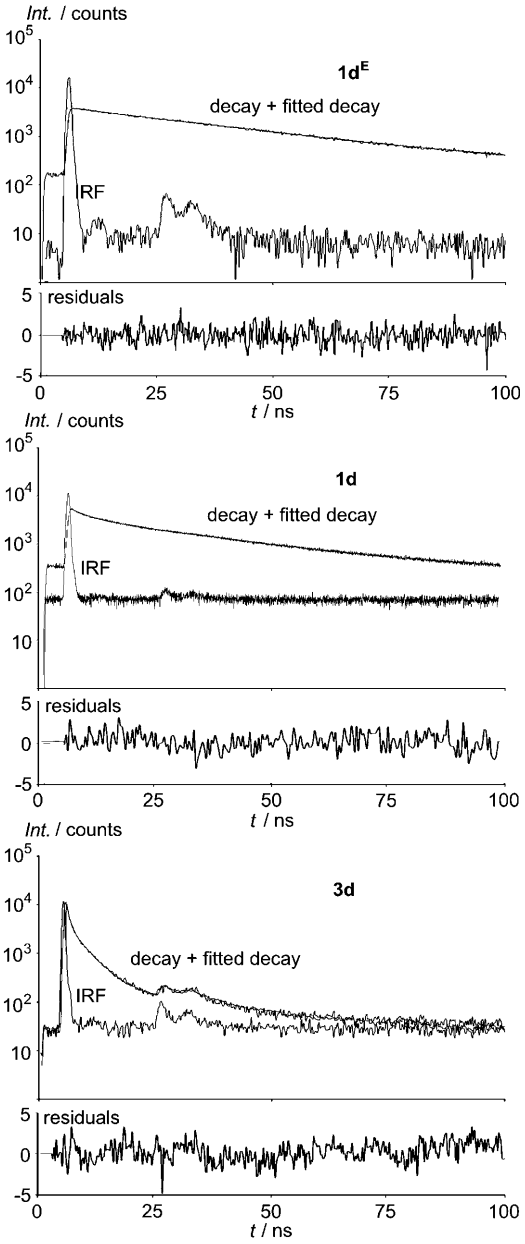

Figure 10. Decay of **1d**^{E} (top) and **1d** (middle) and **3d** (bottom); IRF = instrument response function.

λ_{exc} = 500 nm, Figure 10). Thus we ascribe the first component τ_1 to the usual decay of the substituted heteroleptic $[Ru(tpy)_2]^{2+}$ chromophore and the second shorter component τ_2, which is also found for **2a–2d** and **3a–3f** (τ_2 = 2–4 ns), to a decay pathway established by the acid functionality. Tentatively, this rapid decay pathway can be assumed to be a proton transfer in the excited state, which occurs along hydrogen bonds[49] as aggregation of carboxylic acids to rings or chains through hydrogen bonds (Scheme 3) is prevalent in solution.[50]

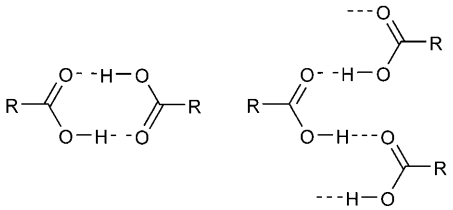

Scheme 3. Aggregation modes of carboxylic acids in solution: ring motif (left) and chain motif (right).

A third component τ_3 is observed ($\tau_3 \approx 1$ ns) when the dyads are excited at the respective chromophore absorption maxima; for example, the coumarin derivatives **2b** and **3b** and the anthracene conjugate **3e** show a third decay component when excited at 370 nm, while the dialkylamino-substituted coumarin derivatives **3c** and **3d** possess a third component when excited at 450 nm, as well as when excited at 500 nm (Table 4, Figure 10). This finding is likely due to the fact that the dialkylamino-substituted coumarin moieties themselves absorb at 500 nm and their residual fluorescence decay can be observed. A prolongation of the ^{3}MLCT lifetime of **3e** due to equilibration of anthracene and MLCT triplet states was not observed, in contrast to the anthracene conjugates prepared by Hanan and Campagna.[22,23] Again, this might be due to an unfavourable relative orientation of the chromophores.

DFT modelling of 2a–2d and 3a–3f: To gain insight into the donor and acceptor features of the building blocks of the dyads the geometries of all conjugates **2a–2d** and **3a–3f** were optimised by DFT methods (B3LYP, LANL2DZ, see Supporting Information). In all cases the individual bond lengths and angles are within the expected ranges. Of particular interest is the intramolecular hydrogen bond in coumarin derivatives **2b** and **3b–3d**, suggested by NMR spectroscopy, which is also reproduced by the calculations (O···H distance 1.74–1.91 Å). In the minimum structures this hydrogen

bond causes the plane of the coumarin chromophore to be coplanar to the terpyridine plane to which it is attached, even when a glycine spacer is inserted in between. The coplanarity is illustrated in Figure 11 for **2b** and **3b**.

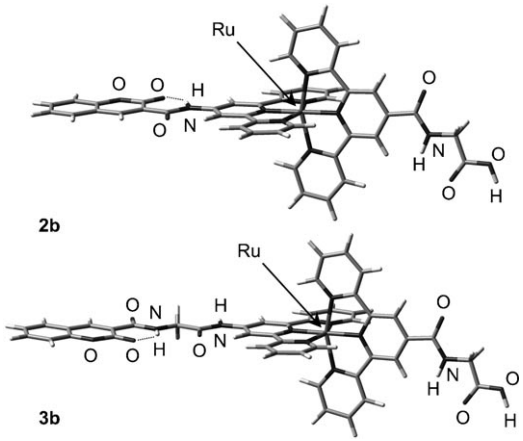

Figure 11. Side view of DFT optimised **2b** and **3b**.

In dyads **2c**, **3e** and **3f** the organic dye is calculated to be oriented in a non-coplanar fashion relative to the terpyridine plane. However, in **2c** and **3f** the organic chromophore should be able to rotate easily around C–C single bonds such that the full conformational space of relative orientations is available. On the other hand, the anthracene derivative **3e** with a directly linked chromophore is sterically quite encumbered, possibly preventing a free rotation of the anthracene moiety. The preferred orientation of the anthracene unit relative to the bis(terpyridine)ruthenium moiety might be less favourable for energy-transfer processes, which might account for the lower energy-transfer efficiency observed for **3e** (vide supra).

The frontier molecular Kohn–Sham orbitals of all dyads were calculated and a graphical representation of relevant orbitals of **3b** is displayed in Figure 12, while a schematic energy diagram for all dyads is depicted in Figure 13.

The mainly metal-centred t_{2g} orbitals are found around −11 eV, the corresponding antibonding e_g set is placed in the region 4.5–5.5 eV. The acceptor orbitals of the MLCT absorption, the π*(tpy) molecular orbitals, lie around −7.7 eV, well below the e_g orbitals. Both the metal t_{2g} and the ligand π*(tpy) orbitals are found at rather constant energy, suggesting that these orbitals are almost unaffected by the organic chromophore, which is also evident from the MO compositions of the respective orbitals (Figure 12). This finding is in accordance with the observations that the MLCT absorption band is found constantly at $\lambda_{max}=490$ nm (Table 2) and that a constant $Ru^{II/III}$ redox potential (Table 1) is observed throughout the series. Relevant π and π* molecular orbitals of the different chromophores in the dyads are also found. They are almost exclusively centred on the chromophores without significant participation of the terpyridine ligands or the ruthenium ion, suggesting electronically isolated chromophores. To further validate the DFT calculations and resulting interpretations the energy difference $\Delta E_{calcd}=E[\pi^*(\text{chromophore})]-E[\pi(\text{chromophore})]$ is plotted against the experimental absorption π→π* absorption band ΔE_{obs} (Figure 14).

Given that an orbital energy difference is only a very crude approximation of energy differences of electronic states the correlation is reasonably good. Thus the DFT calculations corroborate that in the ground state the ruthenium chromophore is electronically decoupled from the organic chromophore.

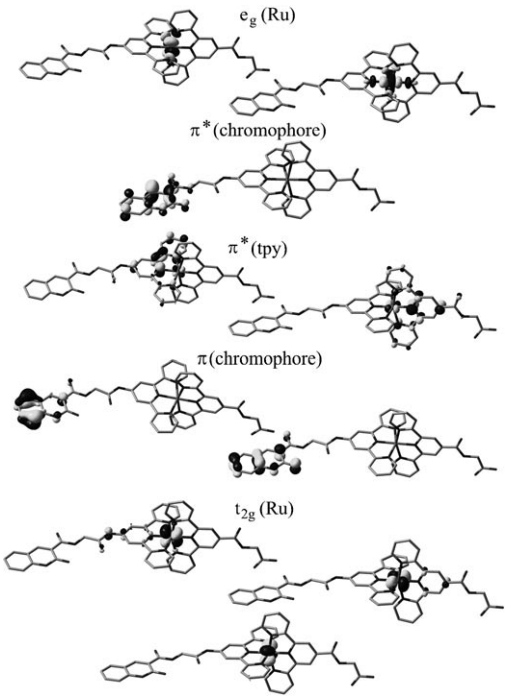

Figure 12. Calculated molecular Kohn–Sham orbitals of **3b** (hydrogen atoms omitted for clarity, isosurface at 0.06 au).

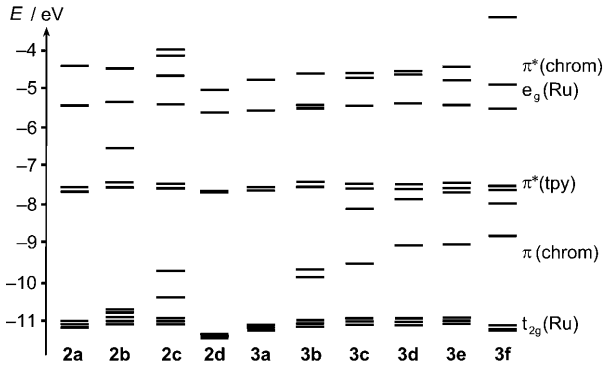

Figure 13. MO scheme of **2a–d** and **3a–f**.

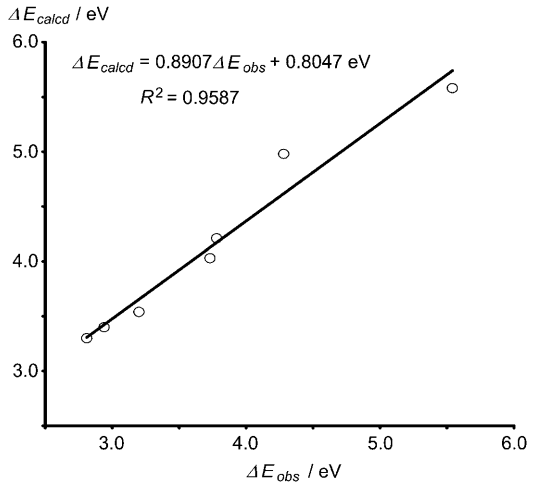

Figure 14. Correlation of the chromophore centred π/π^* energy gap and the experimental absorption maximum of the chromophore.

Conclusion

Solid-phase peptide synthesis methods have been developed and employed to selectively assemble bis(terpyridine)ruthenium(II) acceptor units and organic dyes through amide linkages with and without glycine spacers between the two chromophores. The artificial amino acid **1d** is incorporated into the dyads through amide bonds as the ruthenium-containing building block, while the organic chromophores are introduced either as acid chlorides or activated benzotriazole esters. Activation by acid chlorides is mandatory for coupling with the weakly nucleophilic amino group of **1d**, while coupling to aliphatic amino groups of glycine units requires only PyBOP activation. Microwave irradiation accelerates the solid-phase reactions in some instances. The synthetic method developed yields enough material to allow investigation of the identity and purity of the dyads (NMR, IR, ESI) as well as screening of electrochemical and photophysical properties (absorption, steady-state and time-resolved emission).

Electrochemical data, absorption spectra and DFT calculations of the dyads suggest that in the ground state the building blocks of the dyads are electronically isolated. Energy-transfer processes were shown to occur in the excited dyads as judged from quenched dye fluorescence, excitation spectra and excited-state lifetimes.

The synthetic protocol and screening method developed demonstrates a way towards the realisation of more elaborate multichromophore systems, which could prove useful in (bio-) sensing applications, light-to-chemical energy conversion systems and enhanced photovoltaic cells based on dye sensitisation.

Experimental Section

General procedures: Chemicals were obtained from commercial suppliers and used without further purification. Bis(terpyridine)ruthenium(II) complex **1d** was synthesised as reported.[27] TentaGel-Wang resins and Fmoc-Gly-OH were purchased from IRIS Biotech. Acid chlorides were prepared from the corresponding carboxylic acids according to a literature procedure.[37] For the solid-phase reactions a flask with a nitrogen inlet and a coarse porosity fritted glass filter that allows addition and removal of reagents and solvents without exposure of the resin to the atmosphere was used. Microwave accelerated reactions were conducted in heavy-walled glass vials sealed with aluminium crimp caps fitted with a silicon septum. The inner diameter of the vial filled to the height of 8 cm was 1 cm. Microwave heating was performed in a Discover Benchmate Plus (CEM Synthesis) single-mode microwave cavity producing continuous irradiation at 2.455 GHz with 100 W (max. power). Reaction mixtures were stirred with a magnetic stir bar during irradiation. Temperature and irradiation power were monitored during the course of the reaction. IR spectra were recorded on a BioRad Excalibur FTS 3000 spectrometer with caesium iodide disks. UV/Vis spectra were recorded on a Perkin Elmer Lambda 19 in 1.0 cm cells (Hellma, suprasil). Electrospray mass spectra were recorded with a Finnigan TSQ 700 triple–quadrupole or a Q-Tof Ultima API mass spectrometer (Micromass/Waters, ESI) with analyte solutions in acetonitrile. NMR spectra were obtained on a Bruker Avance DPX 200 (200 MHz, ^{1}H) or a Bruker Avance II 400 (400 MHz, ^{1}H) at 30 °C. Chemical shifts (δ) are reported with respect to residual solvent peaks as internal standards: CD_3CN $\delta(^1H) = 1.94$ ppm, $\delta(^{13}C) = 1.2$, 117.7 ppm. Cyclic voltammetry was performed on a Metrohm "Universal Mess- und Titriergefaess", Metrohm GC electrode RDE 628, platinum electrode, SCE electrode, Princeton Applied Research potentiostat Model 273; in 0.1 M nBu$_4$NB(C$_6$F$_5$)$_4$/CH_3CN. Potentials are given relative to that of SCE. Emission spectra were recorded on a Varian Cary Eclipse spectrometer. Quantum yields were determined by comparing the areas under the emission spectra on an energy scale [cm^{-1}] recorded for optically matched solutions of the samples and the reference ($\phi([Ru(bpy)_3]^{2+}) = 0.062$ in CH_3CN);[51] experimental uncertainty 15%. Luminescence lifetimes were determined on a PicoQuant FluoTime 100 time-correlated single-photon counting unit. Lifetimes were extracted from the decay curve by an iterative reconvolution fitting routine with nonlinear error minimisation using the FluoFit Software. Criteria for the best fit were the values of χ^2; experimental uncertainty 10%. Density functional calculations were carried out with the Gaussian 03/DFT[52] series of programs. The B3LYP formulation of density functional theory was used employing the LANL2DZ basis set.[52]

Synthesis of TentaGel-Gly-⟨Ru⟩-NH$_2$: TentaGel S Wang (0.5 g, loading 0.29 mmol g^{-1}, particle size 90 μm) was soaked in absolute dichloromethane (20 mL) in a 100 mL SPPS flask. Pyridine (0.2 mL) and Fmoc-Gly-Cl[37] (94 mg, 0.29 mmol, 2 equiv) were added and the mixture was shaken in an overhead shaker for 2 h. The solution was filtered and the resin was washed twice with dichloromethane (15 mL). The whole procedure was repeated once (double coupling). Loading with Gly-Fmoc was determined by UV absorption of cleaved Fmoc at 290 nm.[40] Fmoc was removed by addition of a CH_2Cl_2/piperidine mixture (5:1, 15 mL) and shaking for 30 min. The ruthenium building block **1d** (175 mg, 0.19 mmol, 1.3 equiv) was activated by the action of pyridine (0.2 mL) and PyBOP (PyBOP = (benzotriazol-1-yloxy)tripyrrolidinophosphonium hexafluorophosphate; 119 mg, 0.23 mmol, 1.5 equiv) in absolute acetonitrile (15 mL) for 12 h. This mixture was added to the TentaGel-Gly-NH$_2$ resin and the suspension was shaken for 12 h. After filtration the resin was washed three times with acetonitrile (15 mL) and three times with dichloromethane (15 mL) and dried in vacuo giving a deep red resin.

General cleavage procedure: The product was cleaved from the resin by addition of neat TFA (10 mL) and shaking the suspension for 45 min. The deep red TFA solution was collected by filtration and the resin was washed once with acetonitrile (10 mL). The combined solutions were taken to dryness in vacuo. The residue was dissolved in acetonitrile (2 mL), water (30 mL) was added and the product was precipitated by

addition of NH_4PF_6 (50 mg, 0.31 mmol, 2.1 equiv) dissolved in water (5 mL).

Synthesis of 2a: Acetyl chloride (0.04 mL, 34 mg, 0.44 mmol, 3 equiv) and pyridine (0.2 mL) were dissolved in dichloromethane (15 mL) and the solution was poured to the resin TentaGel-Gly-⟨Ru⟩-NH_2. After shaking for 12 h, the suspension was filtered and the resin was washed three times with dichloromethane (15 mL). Complex **2a** was obtained as a red powder (123 mg, 0.121 mmol, 80%) employing the general cleavage procedure. ESI-MS: *m/z* (%): 724.1 (13) $[M]^+$, 362.5 (100) $[M]^{2+}$; HR-MS: *m/z* calcd (%) for $C_{35}H_{28}N_8O_4Ru^{2+}$: 363.06329, found: 363.06356; IR (CsI): $\tilde{\nu}$ = 3442 (OH, NH), 3084 (CH_{aryl}), 2933 (CH_{alkyl}), 1709 (C=O), 1675 (amide I), 1530 (amide II), 1590 (C=N, C=C), 1249 (C−O), 840 cm^{-1} (PF); elemental analysis calcd (%) for $C_{35}H_{28}F_{12}N_8O_4P_2Ru{\cdot}2\,H_2O$ (1015.65): C 39.97, H 3.07, N 10.65; found: C 39.77, H 3.19, N 10.47.

Synthesis of 2b: Coumarin-3-carboxylic chloride[37] (100 mg, 0.48 mmol, 3.2 equiv) and pyridine (0.2 mL) were dissolved in dichloromethane (15 mL) and the solution was poured to the resin TentaGel-Gly-⟨Ru⟩-NH_2. After shaking for 12 h, the suspension was filtered and the resin was washed three times with dichloromethane (15 mL). Complex **2b** was obtained as a red powder (138 mg, 0.12 mmol, 80%), by employing the general cleavage procedure with recrystallisation by addition of diethyl ether (30 mL) to a solution of **2b** in acetonitrile (2 mL). ESI-MS: *m/z* (%): 429.0 (100) $[M]^{2+}$; HR-MS: *m/z* calcd (%) for $C_{43}H_{30}N_8O_6Ru^{2+}$: 428.06603; found: 428.06608. IR (CsI): $\tilde{\nu}$ = 3447 (OH, NH), 3085 (CH_{aryl}), 2932 (CH_{alkyl}), 1722 (C=O), 1667 (amide I), 1530 (amide II), 1571 (C=N, C=C), 1233 (C−O), 843 cm^{-1} (PF); elemental analysis calcd (%) for $C_{43}H_{32}F_{12}N_8O_6P_2Ru{\cdot}2.5\,Et_2O$ (1147.76): C 47.75, H 4.31, N 8.41; found: C 48.26, H 4.04, N 8.62.

Synthesis of 2c: Naphthalen-1-yl-acetyl chloride[37] (100 mg, 0.48 mmol, 3.2 equiv) and pyridine (0.2 mL) were dissolved in dichloromethane (15 mL) and the solution was poured to the resin TentaGel-Gly-⟨Ru⟩-NH_2. After shaking for 12 h, the suspension was filtered and the resin was washed three times with dichloromethane (15 mL). Complex **2c** was obtained as a red powder (126 mg, 0.11 mmol, 73%) by employing the general cleavage procedure, with recrystallisation by addition of diethyl ether (30 mL) to a solution of **2c** in acetonitrile (2 mL). ESI-MS: *m/z* (%): 851.1 (42) $[M]^+$, 426.0 (100) $[M]^{2+}$; HR-MS: *m/z* calcd (%) for $C_{45}H_{34}N_8O_4Ru^{2+}$: 426.08676; found: 426.08686; IR (CsI): $\tilde{\nu}$ = 3445 (OH, NH), 3073 (CH_{aryl}), 2933 (CH_{alkyl}), 1712 (C=O), 1666 (amide I), 1526 (amide II), 1594 (C=N, C=C), 1219 (C−O), 842 cm^{-1} (PF); elemental analysis calcd (%) for $C_{45}H_{34}F_{12}N_8O_4P_2Ru{\cdot}2\,CH_3CN$ (1141.80): C 48.09, H 3.29, N 11.44; found: C 48.16, H 3.46, N 11.10.

Synthesis of 2d: Trifluoroacetyl chloride[37] (50 mg, 0.38 mmol, 2.5 equiv) and pyridine (0.2 mL) were dissolved in dichloromethane (15 mL) and the solution was poured to the resin TentaGel-Gly-⟨Ru⟩-NH_2. After shaking for 12 h, the suspension was filtered and the resin was washed three times with dichloromethane (15 mL). Complex **2d** was obtained as a red powder (128 mg, 0.12 mmol, 80%) by employing the general cleavage procedure. ESI-MS: *m/z* (%): 779.1 (19) $[M]^+$, 390.0 (100) $[M]^{2+}$; HR-MS: *m/z* calcd (%) for $C_{35}H_{25}F_3N_8O_4Ru^{2+}$: 390.04916; found: 390.04947; IR (CsI): $\tilde{\nu}$ = 3451 (OH, NH), 3061 (CH_{aryl}), 2927 (CH_{alkyl}), 1733 (C=O), 1663 (amide I), 1538 (amide II), 1614 (C=N, C=C), 1226 (C−O), 837 cm^{-1} (PF); elemental analysis calcd (%) for $C_{35}H_{25}F_{15}N_8O_4P_2Ru{\cdot}2\,NH_4PF_6$ (1069.62): C 30.12, H 2.38, N 10.04; found: C 30.56, H 2.78, N 9.55.

Synthesis of 3f and TentaGel-Gly-⟨Ru⟩-Gly-NH_2, respectively: Fmoc-Gly-Cl[37] (100 mg, 0.32 mmol, 2 equiv) and pyridine (0.02 mL) were dissolved in THF (8 mL) and the solution was poured to the resin TentaGel-Gly-⟨Ru⟩-NH_2 in a microwave vessel. The suspension was heated in a microwave synthesiser to 80 °C for 1 h. The suspension was filtered and the resin was washed three times with dichloromethane, twice with ethyl acetate and again three times with dichloromethane (15 mL each). Complex **3f** was obtained as a red powder (150 mg, 0.12 mmol, 80%) by employing the general cleavage procedure. ESI-MS: *m/z* (%): 481.6 (100) $[M]^{2+}$; HR-MS: *m/z* calcd (%) for $C_{50}H_{39}N_9O_6Ru^{2+}$: 481.60329; found: 481.60285; IR (CsI): $\tilde{\nu}$ = 3432 (OH, NH), 3075 (CH_{aryl}), 2927 (CH_{alkyl}), 1718 (C=O), 1659 (amide I), 1530 (amide II), 1603 (C=N, C=C), 1226 (C−O), 842 cm^{-1} (PF); elemental analysis calcd (%) for $C_{50}H_{39}F_{12}N_9O_6P_2Ru{\cdot}H_2O$ (1252.90): C 47.25, H 3.25, N 9.92; found: C 47.12, H 3.72, N 9.63.

Fmoc was removed from TentaGel-Gly-⟨Ru⟩-Gly-Fmoc by addition of a CH_2Cl_2/piperidine mixture (5:1, 15 mL) and shaking for 30 min. The resin was washed three times with dichloromethane and dried in vacuo.

Synthesis of 3a: Acetyl chloride (0.04 mL, 34 mg, 0.44 mmol, 3 equiv) and pyridine (0.2 mL) were dissolved in dichloromethane (15 mL) and the solution was poured to the resin TentaGel-Gly-⟨Ru⟩-Gly-NH_2. After shaking for 12 h, the suspension was filtered and the resin was washed three times with dichloromethane (15 mL). Complex **3a** was obtained as a red powder (115 mg, 0.11 mmol, 73%) by employing the general cleavage procedure. ESI-MS: *m/z* (%): 391.6 (100) $[M]^{2+}$; HR-MS: *m/z* calcd (%) for $C_{37}H_{31}N_9O_5Ru^{2+}$: 391.57402; found: 391.57425; IR (CsI): $\tilde{\nu}$ = 3445 (OH, NH), 3062 (CH_{aryl}), 2931 (CH_{alkyl}), 1717 (C=O), 1652 (amide I), 1534 (amide II), 1601 (C=N, C=C), 1229 (C−O), 842 cm^{-1} (PF); elemental analysis calcd (%) for $C_{37}H_{31}F_{12}N_9O_5P_2Ru{\cdot}1.5\,H_2O$ (1072.70): C 40.41, H 3.12, N 11.46; found: C 40.80, H 3.40, N 11.06.

Synthesis of 3b: Coumarin-3-carboxylic acid (100 mg, 0.48 mmol, 3.2 equiv) and pyridine (0.2 mL) were dissolved in dichloromethane (15 mL), and the mixture was activated by addition of PyBOP (250 mg, 0.48 mmol, 3.2 equiv) and stirring for 12 h. The solution was poured to the resin TentaGel-Gly-⟨Ru⟩-Gly-NH_2. After shaking for 12 h, the suspension was filtered and the resin was washed three times with dichloromethane (15 mL). Complex **3b** was obtained as a red powder (111 mg, 0.09 mmol, 62%) by employing the general cleavage procedure. ESI-MS: *m/z* (%): 456.5 (100) $[M]^{2+}$; HR-MS: *m/z* calcd (%) for $C_{45}H_{33}N_9O_7Ru^{2+}$: 456.57676; found: 456.57686; IR (CsI): $\tilde{\nu}$ = 3430 (OH, NH), 3078 (CH_{aryl}), 2931 (CH_{alkyl}), 1719 (C=O), 1655 (amide I), 1526 (amide II), 1608 (C=N, C=C), 1230 (C−O), 842 cm^{-1} (PF); elemental analysis calcd (%) for $C_{45}H_{33}F_{12}N_9O_7P_2Ru{\cdot}C_5H_5N$ (1202.80): C 46.85, H 2.99, N 10.93; found: C 46.62, H 3.03, N 10.93.

Synthesis of 3c: 7-Diethyamino-coumarin-3-carboxylic acid (100 mg, 0.36 mmol, 2.4 equiv) and pyridine (0.2 mL) were dissolved in dichloromethane (15 mL), and the mixture was activated by addition of PyBOP (187 mg, 0.36 mmol, 2.4 equiv) and and stirring for 12 h. The solution was poured to the resin TentaGel-Gly-⟨Ru⟩-Gly-NH_2. After shaking for 12 h, the suspension was filtered and the resin was washed three times with dichloromethane (15 mL). Complex **3c** was obtained as a red powder (90 mg, 0.07 mmol, 47%) by employing the general cleavage procedure. ESI-MS: *m/z* (%): 492.1 (100) $[M]^{2+}$; HR-MS: *m/z* calcd (%) for $C_{49}H_{42}N_{10}O_7Ru^{2+}$: 492.11401; found: 492.11358; IR (CsI): $\tilde{\nu}$ = 3447 (OH, NH), 3076 (CH_{aryl}), 2928 (CH_{alkyl}), 1702 (C=O), 1615 (amide I), 1516 (amide II), 1583 (C=N, C=C), 1227 (C−O), 841 cm^{-1} (PF); elemental analysis calcd (%) for $C_{49}H_{42}F_{12}N_{10}O_7P_2Ru$ (1273.92): C 46.20, H 3.32, N 10.99; found: C 46.46, H 3.59, N 11.01.

Synthesis of 3d: Coumarin343 (100 mg, 0.33 mmol, 2.2 equiv) and pyridine (0.2 mL) were dissolved in dichloromethane (15 mL), and the mixture was activated by addition of PyBOP (172 mg, 0.33 mmol, 2.2 equiv) and and stirring for 12 h. The solution was poured to the resin TentaGel-Gly-⟨Ru⟩-Gly-NH_2. After shaking for 12 h, the suspension was filtered and the resin was washed three times with dichloromethane (15 mL). Complex **3d** was obtained as a red powder (140 mg, 0.11 mmol, 72%) by employing the general cleavage procedure. ESI-MS: *m/z* (%): 504.0 (100) $[M]^{2+}$; HR-MS: *m/z* calcd (%) for $C_{51}H_{42}N_{10}O_7Ru^{2+}$: 504.11416; found: 504.11383; IR (CsI): $\tilde{\nu}$ = 3445 (OH, NH), 3093 (CH_{aryl}), 2937 (CH_{alkyl}), 1693 (C=O, amide I), 1521 (amide II), 1613 (C=N, C=C), 1220 (C−O), 842 cm^{-1} (PF); elemental analysis calcd (%) for $C_{51}H_{42}F_{12}N_{10}O_7P_2Ru$ (1297.94): C 47.19, H 3.26, N 10.79; found: C 47.34, H 3.50, N 10.85.

Synthesis of 3e: Anthracene-2-carboxylic acid (100 mg, 0.45 mmol, 3 equiv) and DCC (120 mg, 0.59 mmol, 3.9 equiv) were dissolved in THF (15 mL) and stirred for 2 h. HOBt (79 mg, 0.59 mmol, 3.9 equiv) was added and the mixture stirred for further 2 h. After filtration the solution was poured to the resin TentaGel-Gly-⟨Ru⟩-Gly-NH_2. After shaking for 12 h, the suspension was filtered and the resin was washed three times with dichloromethane (15 mL). Complex **3e** was obtained as a red powder (60 mg, 0.05 mmol, 33%) by employing the general cleavage procedure. ESI-MS: *m/z* (%): 472.6 (100) $[M]^{2+}$; HR-MS: *m/z* calcd (%) for $C_{50}H_{37}N_9O_5Ru^{2+}$: 472.59801; found: 472.59754; IR (CsI): $\tilde{\nu}$ = 3444 (OH,

NH), 3069 (CH_{aryl}), 2927 (CH_{alkyl}), 1721 (C=O), 1652 (amide I), 1526 (amide II), 1604 (C=N, C=C), 1225 (C−O), 842 cm^{-1} (PF); elemental analysis calcd (%) for $C_{50}H_{37}F_{12}N_9O_5P_2Ru\cdot H_2O$ (1234.88): C 47.93, H 3.14, N 10.06; found: C 48.30, H 3.91, N 9.74.

Acknowledgements

This work was supported by the Deutsche Forschungsgemeinschaft (grant no. HE 2778/5-1). K.H. gratefully acknowledges a Heisenberg fellowship (grant no. HE 2778/4-1) from the Deutsche Forschungsgemeinschaft.

[1] E. A. Medlycott, G. S. Hanan, *Coord. Chem. Rev.* **2006**, *250*, 1763–1782.
[2] J. G. Vos, J. M. Kelly, *Dalton Trans.* **2006**, 4869–4883.
[3] M. Grätzel, *Inorg. Chem.* **2005**, *44*, 6841–6851.
[4] F. Gao, Y. Wang, D. Shi, J. Zhang, M. Wang, X. Jing, R. Humphry-Baker, P. Wang, S. M. Zakeeruddin, M. Grätzel, *J. Am. Chem. Soc.* **2008**, *130*, 10720–10728.
[5] H. Hofmeier, U. S. Schubert, *Chem. Soc. Rev.* **2004**, *33*, 373–399.
[6] C. Siegers, J. Hohl-Ebinger, B. Zimmermann, U. Würfel, R. Mülhaupt, A. Hinsch, R. Haag, *ChemPhysChem* **2007**, *8*, 1548–1556.
[7] F. Felix, J. Ferguson, H. U. Güdel, A. Ludi, *J. Am. Chem. Soc.* **1980**, *102*, 4096–4102.
[8] M. I. J. Polson, F. Loiseau, S. Campagna, G. S. Hanan, *Chem. Commun.* **2006**, 1301–1303.
[9] M. I. J. Polson, E. A. Medlycott, G. S. Hanan, L. Mikelsons, N. J. Taylor, N. Watanabe, Y. Tanaka, F. Loiseau, R. Passalacqua, S. Campagna, *Chem. Eur. J.* **2004**, *10*, 3640–3648.
[10] R. Passalacqua, F. Loiseau, S. Campagna, Y.-Q. Fang, G. S. Hanan, *Angew. Chem.* **2003**, *115*, 1646–1649; *Angew. Chem. Int. Ed.* **2003**, *42*, 1608–1611.
[11] E. A. Medlycott, G. S. Hanan, *Chem. Soc. Rev.* **2005**, *34*, 133–142.
[12] J.-P. Sauvage, J.-P. Collin, J.-C. Chambron, S. Guillerez, C. Coudret, *Chem. Rev.* **1994**, *94*, 993–1019.
[13] M. Maestri, N. Armaroli, V. Balzani, E. C. Constable, A. M. W. Cargill Thompson, *Inorg. Chem.* **1995**, *34*, 2759–2767.
[14] M. Abrahamsson, H. Wolpher, O. Johansson, J. Larsson, M. Kritikos, L. Eriksson, P.-O. Norrby, J. Bergquist, L. Sun, B. Åkermark, L. Hammerström, *Inorg. Chem.* **2005**, *44*, 3215–3225.
[15] H. J. Bolink, L. Capelli, E. Coronado, P. Gaviña, *Inorg. Chem.* **2005**, *44*, 5966–5968.
[16] U. S. Schubert, H. Hofmeier, G. R. Newkome, *Modern Terpyridine Chemistry*, Wiley-VCH **2006**.
[17] F. Odobel, H. Zabri, *Inorg. Chem.* **2005**, *44*, 5600–5611.
[18] G. J. Wilson, A. Launikonis, W. H. F. Sasse, A. W.-H. Mau, *J. Phys. Chem. A* **1997**, *101*, 4860–4866.
[19] D. S. Tyson, F. N. Castellano, *Inorg. Chem.* **1999**, *38*, 4382–4383.
[20] T. Akasaka, T. Mutai, J. Otsuki, K. Araki, *Dalton Trans.* **2003**, 1537–1544.
[21] J. Larson, F. Puntoriero, T. Pascher, N. McClenaghan, S. Campagna, E. Åkesson, V. Sundström, *ChemPhysChem* **2007**, *8*, 2643–2651.
[22] J. Wang, Y.-Q. Fang, L. Bourget-Merle, M. I. J. Polson, G. S. Hanan, A. Juris, F. Loiseau, S. Campagna, *Chem. Eur. J.* **2006**, *12*, 8539–8548.
[23] E. A. Medlycott, G. S. Hanan, F. Loiseau, S. Campagna, *Chem. Eur. J.* **2007**, *13*, 2837–2846.
[24] W. H. Soine, C. E. Guyer, F. F. Knapp, Jr., *J. Med. Chem.* **1984**, *27*, 803–806.
[25] K. J. Kise, Jr, B. E. Bowler, *Inorg. Chem.* **2002**, *41*, 379–386.
[26] B. M. Bishop, D. G. McCafferty, B. W. Erickson, *Tetrahedron* **2000**, *56*, 4629–4638.
[27] K. Heinze, K. Hempel, M. Beckmann, *Eur. J. Inorg. Chem.* **2006**, 2040–2050.
[28] T. Okamura, T. Iwarnura, S. Seno, H. Yamamoto, N. Uyeama, *J. Am. Chem. Soc.* **2004**, *126*, 15972–15973.
[29] K. Heinze, M. Beckmann, K. Hempel, *Chem. Eur. J.* **2008**, *14*, 9468–9480.
[30] N. Metzler-Nolte, *Chimia* **2007**, *61*, 736–741.
[31] G. Dirscherl, B. König, *Eur. J. Org. Chem.* **2008**, 597–634.
[32] S. P. Mulcahy, S. Li, R. Korn, X. Xie, E. Meggers, *Inorg. Chem.* **2008**, *47*, 5030–5032.
[33] M. S. Robillard, A. R. P. M. Valentijn, M. J. Meeuwenoord, G. A. van der Marel, J. H. van Boom, J. Reedijk, *Angew. Chem.* **2000**, *112*, 3226–3229; *Angew. Chem. Int. Ed.* **2000**, *39*, 3096–3099.
[34] N.-M. Hsu, W.-R. Li, *Angew. Chem.* **2006**, *118*, 4244–4248; *Angew. Chem. Int. Ed.* **2006**, *45*, 4138–4142.
[35] L. Baširič, V. Rapič, N. Metzler-Nolte, *Eur. J. Inorg. Chem.* **2006**, 4019–4021.
[36] K. Heinze, U. Wild, M. Beckmann, *Eur. J. Inorg. Chem.* **2007**, 617–623.
[37] M. Beyermann, M. Bienert, H. Niedrich, L. A. Carpino, D. Sadat-Aalaee, *J. Org. Chem.* **1990**, *55*, 721–728.
[38] E. Bayer, *Angew. Chem.* **1991**, *103*, 117–133; *Angew. Chem. Int. Ed. Engl.* **1991**, *30*, 113–129.
[39] M. Grøtli, C. H. Gotfredsen, J. Rademann, J. Buchardt, A. J. Clark, J. Ø. Duus, M. Meldal, *J. Comb. Chem.* **2000**, *2*, 108–119.
[40] *Fmoc Solid Phase Peptide Synthesis* (Eds.: W. C. Chan, P. D. White), Oxford University Press, Oxford **2000**.
[41] L. A. Carpino, M. Beyermann, H. Wenschuh, M. Bienert, *Acc. Chem. Res.* **1996**, *29*, 268–274.
[42] M. Erdélyi, A. Gogoll, *Synthesis* **2002**, *11*, 1592–1596.
[43] M. Hesse, H. Meier, B. Zeeh, *Spektroskopische Methoden in der organischen Chemie*, Thieme, Stuttgart **1991**.
[44] N. Camire, U. T. Mueller-Westerhoff, W. E. Geiger, *J. Organomet. Chem.* **2001**, *637*, 823–826.
[45] W. W. Mantulin, P.-S. Song, *J. Am. Chem. Soc.* **1973**, *95*, 5122–5129.
[46] I. Aujard, C. Benbrahim, M. Gouget, O. Ruel, J.-B. Baudin, P. Neveu, L. Jullien, *Chem. Eur. J.* **2006**, *12*, 6865–6879.
[47] R. E. Riter, J. R. Kimmel, E. P. Undiks, N. E. Levinger, *J. Phys. Chem. B* **1997**, *101*, 8292–8297.
[48] A. C. Benniston, A. Harriman, P. Li, P. V. Patel, C. A. Sams, *Chem. Eur. J.* **2008**, *14*, 1710–1717.
[49] Y. Nosenko, G. Wiosna-Salyga, M. Kunitski, I. Petkova, A. Singh, W. J. Buma, R. P. Thummel, B. Brutschy, J. Waluk, *Angew. Chem.* **2008**, *120*, 6126–6129; *Angew. Chem. Int. Ed.* **2008**, *47*, 6037–6040.
[50] G. R. Desiraju, *Angew. Chem.* **1995**, *107*, 2541–2558; *Angew. Chem. Int. Ed. Engl.* **1995**, *34*, 2311–2327.
[51] J. V. Caspar, T. J. Meyer, *J. Am. Chem. Soc.* **1983**, *105*, 5583–5590.
[52] Gaussian 03, Revision B.03, M. J. Frisch, G. W. Trucks, H. B. Schlegel, G. E. Scuseria, M. A. Robb, J. R. Cheeseman, J. A. Montgomery, Jr., T. Vreven, K. N. Kudin, J. C. Burant, J. M. Millam, S. S. Iyengar, J. Tomasi, V. Barone, B. Mennucci, M. Cossi, G. Scalmani, N. Rega, G. A. Petersson, H. Nakatsuji, M. Hada, M. Ehara, K. Toyota, R. Fukuda, J. Hasegawa, M. Ishida, T. Nakajima, Y. Honda, O. Kitao, H. Nakai, M. Klene, X. Li, J. E. Knox, H. P. Hratchian, J. B. Cross, C. Adamo, J. Jaramillo, R. Gomperts, R. E. Stratmann, O. Yazyev, A. J. Austin, R. Cammi, C. Pomelli, J. W. Ochterski, P. Y. Ayala, K. Morokuma, G. A. Voth, P. Salvador, J. J. Dannenberg, V. G. Zakrzewski, S. Dapprich, A. D. Daniels, M. C. Strain, O. Farkas, D. K. Malick, A. D. Rabuck, K. Raghavachari, J. B. Foresman, J. V. Ortiz, Q. Cui, A. G. Baboul, S. Clifford, J. Cioslowski, B. B. Stefanov, G. Liu, A. Liashenko, P. Piskorz, I. Komaromi, R. L. Martin, D. J. Fox, T. Keith, M. A. Al-Laham, C. Y. Peng, A. Nanayakkara, M. Challacombe, P. M. W. Gill, B. Johnson, W. Chen, M. W. Wong, C. Gonzalez, and J. A. Pople, Gaussian, Inc., Pittsburgh PA, **2004**.

Received: September 10, 2008
Published online: January 2, 2009

